https://doi.org/10.2352/ISSN.2470-1173.2018.15.COIMG-134

Feature Selection for Material Identification in Spectral CT

Parisa Babaheidarian and David Castañón; Boston University; Boston, MA/U.S.A.

Abstract

Detecting materials of interest in containers using X-ray measurements is a critical problem in aviation security. Conventional X-ray systems obtain single- or dual-energy measurements, which are subsequently processed using computed tomography (CT) to obtain estimates of attenuation properties of different regions. Recently, novel detectors enable the measurement of the X-ray transmission intensities on multiple energy bands, leading to the use of spectral CT to construct additional properties of regions to assist in material identification. In this paper, we discuss the problem of material classification using spectral CT. We introduce a new basis representation which can accurately represent energy-dependent X-ray transmission characteristics in a few dimensions, and propose a class of reconstruction techniques for obtaining features of different regions. We illustrate the advantages of our approach over alternative approaches using different basis representations as well as CT reconstructions in each energy band using simulated spectral CT experiments. Our results illustrate that there are significant advantages to using our basis representation in both detection and material classification performance, particularly in the presence of complex materials or mixtures involving atoms with high atomic number.

Introduction

Automatic material recognition in X-ray CT images has a wide range of applications both for medical and security purposes. In the medical domain, an automatic recognition algorithm helps the radiologist in diagnosis of tumors and pathology in tissues, particularly when the image contrast is poor. In security, automated recognition algorithms assist operators in detection of hazardous materials and reduces the need for human inspections. For the security application, the range of possible materials in bags makes it difficult to separate hazardous materials from regular stream-of-commerce materials.

In order to obtain sufficient information for identifying hazardous materials, security applications often use dual-energy scanners [1–5] that collect attenuation responses for two different excitation spectral energy distributions. The dual energy measurements can be translated using CT techniques to estimates of the effective atomic number and electron density of a region, which can be used to identify the material in the region. This works well with materials that have low effective atomic number, but is less reliable for other materials.

Recently, new classes of photon-counting detectors have enabled the collection of X-ray attenuation responses over several energy spectral distributions simultaneously [6–9], leading to the novel spectral X-ray CT instruments. Such instruments have been used recently for medical applications [8, 10–12], and have shown potential for identifying complex images including contrast agents. This can allow imaging of regions which use more than one contrast agent in the same scan. As an example, a blood pool gadolinium-based contrast agent could be used in combination with a tumor or thrombus-specific bismuth-linked agent without the need for additional scans and radiation exposure [13].

For security applications, PCDs can enhance material recognition by collecting the attenuation responses of the region of interest using multiple energy spectra. This can be used to reconstruction effective attenuation at different average excitation energies, thus providing additional features for material recognition. Alternatively, one can use basis decomposition techniques [1, 4, 5] for representing the energy-dependent linear attenuation coefficients of materials. Typical basis functions used are photoelectric and Compton scattering bases, selected material bases, and basis functions selected from principal component analysis of multiple material linear attenuation coefficients. The multispectral attenuation measurements can be used to reconstruct images of the coefficients of these basis representations, yielding a different set of features for material recognition.

In this paper, we describe multiple approaches for extracting meaningful information from multispectral energy measurements, and using this information for material identification. In addition to conventional approaches based on dual energy imaging techniques, we define a novel basis that is well-suited for representing complex materials with higher effective atomic numbers. We examine the relative performance of these approaches for material identification and for detection of explosives using simulated experiments with multi-spectral CT detectors in tomographic imaging configurations. Our results indicate that there are significant advantages in detection and material recognition performance that result from using our new basis for multispectral CT.

The rest of this paper is organized as follows: first, we review basis decomposition approaches used in dual energy imaging. We subsequently extend these techniques to apply to multispectral CT imaging with more general basis decomposition techniques. We introduce a new basis decomposition using sparse regression that is more suited for representing the energy-dependence of linear attenuation coefficients for materials or mixtures involving higher atomic number atoms. Subsequently, we describe algorithms for using alternative basis functions to reconstruct features of materials at different locations in the image. We then describe a material identification algorithm based on using graph-cut techniques for discrete optimization. We conclude the paper with simulated multispectral CT experiments that compare the performance of different feature extraction approaches using detection and recognition experiments.

This material is based upon work supported by the U.S. Department of Homeland Security, Science and Technology Directorate, Office of University Programs, under Grant Award 2013-ST-061-ED0001. The views and conclusions contained in this document are those of the authors and should not be interpreted as necessarily representing the official policies, either expressed or implied, of the U.S. Department of Homeland Security.

Multispectral CT

We briefly review the basis decomposition approach to dual energy imaging as originally outlined in [1]. Then, we extend these approaches for multispectral CT imaging. For simplicity of exposition, we focus on systems that use photon-counting detectors as the measurement instruments.

Dual Energy Imaging

We briefly review the basis decomposition approach to dual energy imaging as originally outlined in [1]. For simplicity, we focus on systems that use photon-counting detectors. We assume that we have sources i with effective source/detector spectrum denoted by $I_0 W_i(E)$, where I_0 is the total photon flux and $W_i(E)$ denotes the energy weighting function, which can be interpreted as the fraction of photons that have energy E. We assume that this excitation is uniform for each detector.

Assume we are imaging through a volume with energy-dependent and space-dependent linear attenuation coefficient $\mu(\mathbf{r},E)$. Define c_L^i as the received count at i-th PCD at detector L when spectrum i is used with source-detector path $\ell(L)$. We assume a statistical model for the observed counts is a Poisson model with average intensity described below, as

$$c_L^i = \text{Poiss}\left(\int_E W_i(E) I_0 e^{-\int_{\ell(L)} \mu(\mathbf{r},E)\, d\mathbf{r}} dE\right), \quad i = 1,2 \tag{1}$$

In this model, we neglect effects of electronic measurement noise and other small deviations, although our subsequent analysis would be readily extended to include these effects. The observed counts are reported in terms of normalized sinogram values as,

$$y_L^i = -\log\left(\frac{c_L^i}{\int_E W_i(E) I_0 dE}\right) \tag{2}$$

One approach for processing dual energy spectral measurements is to reconstruct an average attenuation $\hat{mu}^i(\mathbf{r})$ for each spectrum i from the normalized observed counts y_L^i for all the tomographic projections L. The two values $\hat{mu}^1(\mathbf{r}), \hat{mu}^2(\mathbf{r})$ reconstructed at each voxel would provide the underlying features for material classification. An alternative approach is to represent the energy-dependent linear attenuation coefficient $\mu(\mathbf{r},E)$ in a basis expansion with two basis functions, as

$$\mu(\mathbf{r},E) = a(\mathbf{r}) f_1(E) + b(\mathbf{r}) f_2(E) \tag{3}$$

where $f_1(E), f_2(E)$ are functions that represent the energy dependence of linear attenuation coefficients. Common basis functions are the photoelectric and Compton (PEC) scatter cross-sections, with the photoelectric basis defined as

$$f_p(E) = \frac{1}{E^3} \tag{4}$$

and the Compton basis is a Klein-Nishina approximation [14] given by

$$f_c(E) = \frac{1+a}{a^2}\frac{2(1+a)}{(1+2a) - \frac{1}{a}\log(1+2a)} + \frac{1}{2a}\log(1+2a) - \frac{1+3a}{(1+2a)^2}, \tag{5}$$

where $a = \frac{E}{C}$ for some constant C which is usually set as $C = 510.999$ keV.

Given a choice of basis functions, sinogram decomposition is used for each pair of detector measurements to linearize the relationship between coefficients and measurements. Using the approximation in (3), we obtain the following expression for at each detector L in terms of the expected measurements:

$$E[c_L^1] = \int_E W_1(E) I_0 e^{-f_1(E)\int_{\ell(L)} a(\mathbf{r})d\mathbf{r} - f_2(E)\int_{\ell(L)} b(\mathbf{r})d\mathbf{r}} dE \tag{6}$$

$$= \int_E W_1(E) I_0 e^{-f_1(E) A_L - f_2(E) B_L} dE \tag{7}$$

$$E[c_L^2] = \int_E W_2(E) I_0 e^{-f_1(E)\int_{\ell(L)} a(\mathbf{r})d\mathbf{r} - f_2(E)\int_{\ell(L)} b(\mathbf{r})d\mathbf{r}} dE \tag{8}$$

$$= \int_E W_2(E) I_0 e^{-f_1(E) A_L - f_2(E) B_L} dE \tag{9}$$

The measurements c_L^1, c_L^2 are noisy estimates of the left-hand side of the above equations. The sinogram decomposition approach first estimates A_L, B_L from the pair of measurements c_L^1, c_L^2 using nonlinear regression or max-likelihood estimation techniques. Given these estimates $\hat{A}_L, \hat{B}_L$, we have the following approximate relationships:

$$\hat{A}_L = \int_{\ell(L)} a(\mathbf{r}) d\mathbf{r} \tag{10}$$

$$\hat{B}_L = \int_{\ell(L)} B(\mathbf{r}) d\mathbf{r} \tag{11}$$

These equations correspond to linear tomographic projections of the coefficient fields $a(\mathbf{r}), b(\mathbf{r})$. Thus, the collection of estimates $\hat{A}_L$ can be processed to reconstruct estimates $\hat{a}(\mathbf{r})$ using tomographic reconstruction techniques. Similarly, the collection $\hat{B}_L$ will generate $\hat{b}(\mathbf{r})$. The values of $\hat{a}(\mathbf{r}), \hat{b}(\mathbf{r})$ form the features that characterize the material at location $\mathbf{r}$.

Extensions to Multispectral CT

The above procedures can be extended to multispectral measurements in a straightforward manner, as follows. Our measurement model is the same as (1), except that the number of spectra I is greater than 2. The direct reconstruction approach processes the collections of measurements y_L^i for each $i \in I$ and obtains an estimate for the average attenuation for that spectrum, as $\hat{\mu}^i(\mathbf{r})$.

The basis expansion approaches can use a larger set of basis functions, with the approximation that $\mu(\mathbf{r},E)$ decomposes as

$$\mu(\mathbf{r},E) = a^1(\mathbf{r}) f_1(E) + a^2(\mathbf{r}) f_2(E) + \ldots + a^K(\mathbf{r}) f_K(E) \tag{12}$$

where $f_k(E))$ are basis functions that represent the energy dependence of linear attenuation coefficients, and $a_K(\mathbf{r})$ are coefficients that represent the expansion of $\mu(\mathbf{r},E)$ in that basis representation. The sinogram decomposition follows in a similar manner to the dual energy decomposition:

$$E[c_L^i] = \int_E W_i(E) I_0 e^{-\sum_{k=1}^K f_k(E)\int_{\ell(L)} a^k(\mathbf{r})d\mathbf{r}} dE$$

$$= \int_E W_i(E) I_0 e^{-\sum_{k=1}^K f_k(E) A_L^k} dE \tag{13}$$

The measurements $c_L^i, i = 1,\ldots,I$ are noisy estimates of the left-hand side of the above equations. The sinogram decomposition approach estimates $A_L^k, k = 1,\ldots,K$ from the set of measurements $c_L^1,\ldots,c_L^I$ using a nonlinear regression technique, which is

well-posed provided $I \geq K$. For each k, the collection of estimates $\hat{A}_L^k$ is processed using tomographic reconstruction techniques to obtain estimate $\hat{a}^k(\mathbf{r})$. The collection of values $\hat{a}^k(\mathbf{r}), k = 1,\ldots,K$ are the features associated with the material in location $\mathbf{r}$.

The fundamental question that remains is the choice of basis functions. A good choice of basis functions is one where the basis functions are linearly independent, and yield good approximation of all of the linear attenuation coefficient functions for the materials of interest. Different choices of basis functions can lead to changes in performance in recognition of materials.

Choice of Basis Functions

In this paper, we evaluate several choices for basis functions to use for multispectral CT imaging. The first choice of basis is the standard photoelectric and Compton basis decomposition used in dual-energy imaging (as in (4),(5)), extended to use multi-spectral measurements. A second choice of basis can be obtained from the principal components of the linear attenuation coefficient functions over a range of energies of interest, as generated for a test group of sample materials. These functions would be independent and orthogonal over the range of energies of interest.

One of the limitations of the photoelectric/Compton (PEC) basis is that the basis functions have a smooth dependence on energy. As such, the PEC basis represents LACs accurately for materials with low effective atomic number. However, they do not represent accurately the linear attenuation coefficients of materials or mixtures that include atoms with K-edges in the X-ray energy region of interest. A K-edge material is a material whose linear attenuation coefficient as a function of energy contains a discontinuity in the relevant energy range, typically $[30-150]$ keV. In security applications, the range of materials of interest is broad, and includes K-edge materials. As an example, Figure 1 displays the LAC of Baratol, a combination of Barium with TNT, that has a K-edge at 38 keV [15].

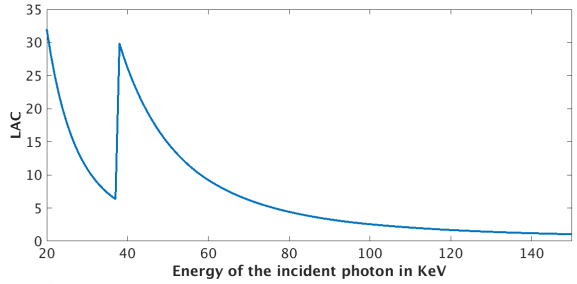

Figure 1: The nominal LAC function of Baratol. The values are obtained from NIST dataset [15].

Figure 2 illustrates the issue with PEC decompositions. The LAC functions of two materials, TNT and Baratol, are plotted in green, and the blue plots with show the least squares reconstruction of LAC values using the PEC basis for the energy range $[30-129]$ keV. The inaccurate fit for Baratol can lead to misclassification when the reconstructed features are the PEC coefficients.

To improve the accuracy of basis representations for complex materials including atoms with K-edges, we introduce a new basis transform, termed SPECK which is a short form for Sparse photoelectric, Compton, and K-edge basis. The first two basis functions in the transform are the photoelectric and Compton basis functions of (4),(5). To these two functions we add the LAC functions of the

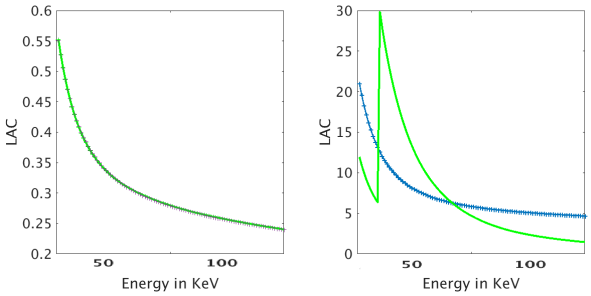

Figure 2: The least squares reconstruction of LAC of two materials using PEC basis transform against their nominal values. From left to right, TNT and Baratol reconstruction results are plotted in blue curves with '+' markers. The solid green plots represent the nominal LAC curves.

atoms that have K-edges in the energy range $[30-130]$ keV. Note that these other basis functions are linearly independent from each other and the first two bases, because they have discontinuities at different energy values. However, the number of basis functions K can be larger than the number of energy bins I, so max-likelihood techniques are no longer adequate estimating the decomposed measurements A_L^k for each detector L using the measurements c_L^i in (13). To accommodate for this, we propose the use of sparse regression, where the goal is to represent accurately the measurements using a small number of nonzero coefficients.

Specifically, define $\underline{A} = [A^1,\ldots,A^K]$ as the vector of coefficients of the SPECK basis used to represent a set of observations, and let $f_k(E)$ be the basis functions in the SPECK basis. Define

$$g^i(\underline{A}) \triangleq \int_E W_i(E) I_0 e^{-\sum_{k=1}^K f_k(E) A^k} dE$$

For each detector L with multispectral energy measurements $c_L^i, i = 1,\ldots,I$, we propose to compute the coefficients $A_L^1,\ldots,A_L^K$ by solving the following optimization problem:

$$[A_L^1,\ldots,A_L^K] = \arg\min_{\underline{A}\geq 0} \sum_{i=1}^{I} (c_L^i - g^i(\underline{A}))^2 + \lambda \sum_{i=1}^{K} |A^i| \qquad (14)$$

for a parameter $\lambda > 0$ that controls the desired level of sparsity in the coefficient vector. Note that the non-negativity constraints in the optimization arise from the choice of basis functions that represent physical processes.

To demonstrate the accuracy of SPECK representation of LAC signals, we have plotted the noise-free reconstruction results, produced by SPECK features, in Figure 3 for a few materials, including two K-edge materials.

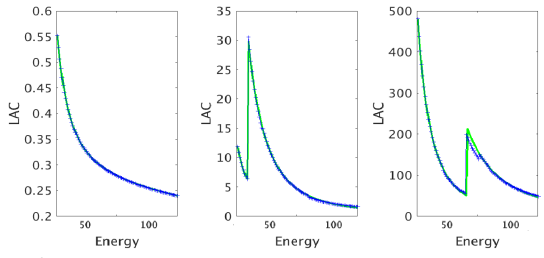

Figure 3: From left to right, reconstructed LAC values using SPECK features against nominal LACs for TNT, Baratol, and Tungsten. The nominal plots are in green and the reconstructed values are plotted in blue.

Given the decomposed measurements $[A_L^1,\ldots,A_L^K]$ for all the detectors L, we use standard tomographic reconstruction techniques to transform these into coefficient images $\hat{a}^k(\mathbf{r})$ for $k=1,\ldots,K$. For the results that follow, we used an iterative reconstruction technique. Let A denote the forward projection operator, let $\mathbf{a}^k$ denote the vector of coefficients $a^k(\mathbf{r})$, and let $\mathbf{y}^k$ denote the vector of decomposed measurements A_L^k for the different detectors L. The reconstructed image $\hat{\mathbf{a}}^k$ is obtained from the following optimization problem:

$$\min_{\mathbf{a}^k\geq 0}\|\mathbf{y}^k - A\mathbf{a}^k\|_2^2 + \lambda\left(\|D_x\mathbf{a}^k\|_2^2 + \|D_y\mathbf{c}_b\|_2^2\right) \tag{15}$$

where D_x and D_y are discrete forward difference operators in spatial coordinates x,y represented as matrices, and parameter λ controls the trade-off between the regularization term and the data fidelity term.

Recognition Algorithms

We formulate the recognition problem as a MAP estimation problem, where the goal is to identify the material in each discrete spatial location $\mathbf{r}$ from a fixed number of possible materials. We assume that our image is composed of N^2 pixels. Our goal in classification is to assign one of a finite number of material labels $m=1,\ldots,M$ to each pixel. Let $\mathbf{a}(i)$ denote the vector of reconstructed features $[a^1(i),\ldots,a^m(i)]$ at pixel i, where these features are coefficients in a basis expansion, or direct reconstructions of average linear attenuation using several spectral measurements.

Assume that we have a dictionary of possible materials, from which we can estimate the statistics of the nominal feature values $a_m^1,\ldots,a_m^k$ for material m given a range of instances of the material. We assume that the coefficient values at pixel m in the image with material class $\ell(m)\in\{1,2,\ldots,|D^r|\}$ are sampled from a multivariate Gaussian distribution with mean vector $\gamma_{\ell(m)}$ and covariance matrix $\Sigma_{\ell(m)}$, i. e.,

$$\mathbf{a}(m)\sim\mathcal{N}\left(\Gamma_{\ell(m)},\Sigma_{\ell(m)}\right), \tag{16}$$

To model the prior distribution of material labels in our MAP formulation, we want to represent the information that our materials have significant extent. To do this, we assume a Potts Markov random field model for the prior distribution of the labels. Specifically, let $\Omega(i)$ denote the neighboring pixels of pixel i, and let $1_{\{\ell_i\neq\ell_j\}}$ denote the indicator function that is 1 if the label ℓ_i of pixel i is the same as the label ℓ_j of pixel j. We formulate the joint segmentation/classification problem given the reconstructed coefficient features as

$$\min_{\ell_i,i\in\{1,\ldots,N^2\}}\sum_{i=1}^{N^2}(\mathbf{a}(i)-\Gamma_{\ell(i)})^T\Sigma_{\ell(i)}^{-1}(\mathbf{a}(i)-\Gamma_{\ell(i)}) + \alpha\sum_{i=1}^{N^2}\sum_{j\in\Omega(i)}1_{\{\ell_i\neq\ell_j\}} \tag{17}$$

The parameter $\alpha>0$ controls the smoothing effect in the Markov random field over the pixels' labels.

The optimization in (17) is a discrete optimization over label classes. Note that the Potts model satisfies metric property, therefore, it induces an objective function with the submodularity property which can be efficiently optimized using α-expansion graph cut algorithm [16]. We solve this optimization using the multi-class α-expansion algorithm [16] which converges to a local optimal solution that is guaranteed to be within a known factor of 2 of the global optimal solution.

Experiments

In this section, we describe the results of simulation experiments using 2-D phantoms containing diverse mixtures of materials. We conduct two classes of experiments: classification experiments where the objective is to identify the material type accurately, and detection experiments, where the objective is to detect whether we group materials into two classes: explosives and non-explosives, and the objective is to determine which class the material is in. For each experiment, we compute the performance achieved using four different sets of features: Photoelectric/Compton (PEC) features, PCA features using the first five principal components learned from the LAC of the dictionary of materials, the SPECK features discussed earlier, and features obtained by direct reconstruction of the average linear attenuation coefficient in each spectral energy bin in the multispectral detectors.

In all experiments, we use a 2-D imaging system imaging an area of $350mm\times 350mm$, which we reconstruct in terms of $1mm^2$ pixels. We use an array of 1000 detectors per view, with detector size $0.75mm$. For tomography, we use 200 views, evenly spaced between 0 and π radians. For detectors, we use photon counting detectors with 10 ideal spectral bands, with width 10 keV, in the energy range $[30-129]$ keV. The source spectrum sends a total of $I=2\times 10^6$ photons per detector, spread out according to the spectrum in Figure 4. The received counts and sinogram values were simulated using equations (1) and (2), with the correction that we lower bounded the sinogram values to be nonnegative.

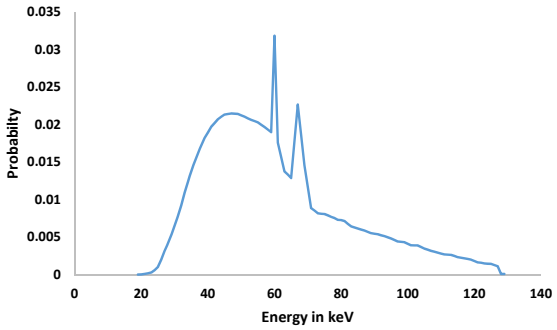

Figure 4: Spectrum of source used in experiments

Classification experiments

The classification experiments used a test set of 67 materials, including several K-edge materials. Using these 67 materials, we generated 80 phantoms, consisting of 3 regions each filled with a different material, randomly selected from the available materials . The energy-dependent linear attenuation coefficients of each material were obtained from NIST reference data [15]. The features extracted from these 80 phantoms were used as training data to learn the parameters of the classification algorithm, namely the means and variances of the Gaussian values of parameters. For test data, we created 20 phantoms with similar structures.

For each of the phantoms, we collected data and formed the

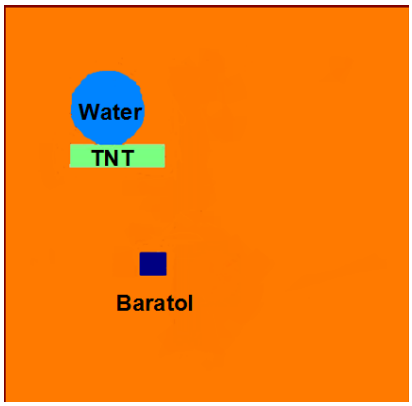

Figure 5: A tested phantom with three regions. The colors represent the true labels.

Algorithm	Average classification accuracy
SPECK	86.7%
PEC	75%
Direct LAC reconstruction	68.3%
PCA (six bases)	61.6%

Table 1: The average classification performance using different features. The average was computed over 20 tested with phantoms with both smooth LAC materials and materials with K-edges.

SPECK, PEC, PCA and the direct LAC reconstruction features using the tomographic approaches described earlier. For each of the test images, we computed the average coefficient vector per material class and its covariance by averaging over the pixels in the strict interior regions of the areas in the phantoms containing this material class.

For the test phantoms, we reconstructed the features for all pixels using the different feature sets , and subsequently used the graph cut segmentation/classification algorithm to assign a label to each pixel. To evaluate the region classification accuracy, we used the ground truth segmentation to compute the number of correctly classified pixels in each region. Then, we assumed that a region is correctly labeled if more than 50% of its pixels are labeled with the correct material label.

Figure 5 displays an example of tested phantoms with three regions including *Water*, *TNT*, and *Baratol* regions. Note that TNT and Baratol are explosives and Baratol has a K-edge in the operating energy range. The background is filled with air.

Table 1 summarizes the average material classification performance over the 20 phantoms in the test data set. Our average results indicate that the classification performance of SPECK is superior to the performance obtained using alternative features.

Detection experiments

In these experiments, we focus on the task of explosive detection which is a binary classification problem. We selected a collection of 80 materials to be included in the experiments, with 40 explosive materials and 40 non-explosive materials. In this collection, 12 K-edge materials were included.

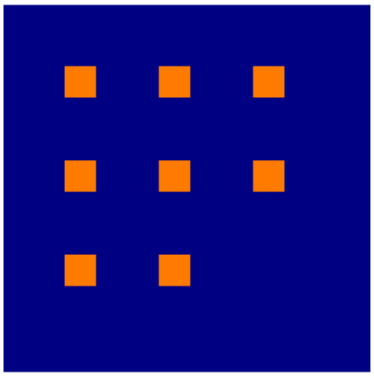

Figure 6: The structure of the template phantom used in the explosive detection evaluation for the tomography model.

Features	$\sigma = 0$	$\sigma = 0.05$	$\sigma = 0.1$
SPECK	99.4%	96.0%	96.0%
PEC	94.1%	90.05%	89.5%
Direct LAC reconstruction	94.1%	88.8%	85.0%
PCA (5 bases)	94.8%	86.0%	83.0%

Table 2: The classification performance on the test data with different levels of distortion to the nominal dictionary, using random forests classifiers with 10 trees.

We generated 100 phantoms of size $350mm \times 350mm$, each of which included four regions with explosive materials and 4 regions with non-explosive materials, randomly selected from the collection of experiments. The regions were $30mm \times 30mm$ each. Figure 6 shows the structure of the template phantom.

These 100 phantoms were used as training data to train a classifier. To create the test data, we created twenty additional phantoms with the same structure as in the training data and randomly filled the regions in each phantom using materials in the experiment. To add additional variability, we perturbed the linear attenuation coefficients of the materials randomly from their nominal values in the test data.

As a classification algorithm, we used a random forest classifier with 10 trees, using the MATLAB TreeBagger function to train and implement the classifier. As before, we built different classifiers for different feature sets (SPECK, PEC, PCA, and Direct LAC), training on the same phantoms for training data. The classification performance was tested on 20 phantoms with different levels of random perturbations of the LACs, corresponding to $\sigma = 0$, $\sigma = 0.05$, and $\sigma = 0.1$, where σ indicates the average deviation from the nominal LAC value used in the test data. Table 2 summarizes the classification results on the test data for all the tested bases. The results illustrate the advantage of using the SPECK basis over the alternative approaches for obtaining accurate detection.

Conclusion

In this paper, we considered the problems of image reconstruction and feature extraction using multispectral imaging systems. The availability of multiple spectral measurements per detector opens

avenues for extracting different types of features for recognition of materials and detection of explosives. We described an approach for extracting features as part of multispectral CT reconstructions using basis expansions of energy-dependent linear attenuation coefficients. We introduced a new basis representation, SPECK, which accurately represents the LAC signal in few dimensions, particularly for materials and mixtures that contain high atomic number atoms.

We evaluated different reconstruction and feature extraction algorithms for multispectral CT for the task of material classification, and evaluated the relative performance of these algorithms on a simulated material classification task. Our results indicate that the SPECK basis representation extracts features that offer significant improvement for material classification. We conducted further experiments on a different task, involving detection of explosives materials. Again, our experiment results indicate significant advantages for using the SPECK basis representation to extract features when compared with the alternative feature extraction techniques.

There are several directions of interest for future investigation. The evaluation results for classification require a priori knowledge of the set of materials considered. We would like to extend this to cases where the materials are unknown. In addition, we would like to validate the results of these papers using data from spectral CT systems with different material mixtures. Finally, we would like to consider new classes of reconstruction algorithms that perform feature reconstruction jointly, as opposed to the independent approach described in this paper.

References

[1] R. Alvarez and A. Macovski, "Energy-selective reconstructions in X-ray computerised tomography," *Physics in medicine and biology*, vol. 21, no. 5, p. 733, 1976.

[2] S. Singh and M. Singh, "Explosives detection systems (EDS) for aviation security," *Signal Processing*, vol. 83, no. 1, pp. 31–55, 2003.

[3] Y. Long and J. A. Fessler, "Multi-material decomposition using statistical image reconstruction for spectral CT," *IEEE transactions on medical imaging*, vol. 33, no. 8, pp. 1614–1626, 2014.

[4] S. G. Azevedo, H. E. Martz, M. B. Aufderheide, W. D. Brown, K. M. Champley, J. S. Kallman, G. P. Robertson, D. Schneberk, I. M. Seetho, and J. A. Smith, "System-independent characterization of materials using dual-energy computed tomography," *IEEE Transactions on Nuclear Science'*, vol. 63, no. 1, 2016.

[5] Z. Ying, R. Naidu, and C. R. Crawford, "Dual energy computed tomography for explosive detection," *Journal of X-Ray Science and Technology*, vol. 14, pp. 235–256, 2006.

[6] E. Frey, K. Taguchi, M. Kapusta, J. Xu, T. Orskaug, I. Ninive, D. Wagenaar, and B. P. B. Tsui, "Microcomputed tomography with a photon-counting X-ray detector," *Proceedings of SPIE*, vol. 6510, p. 65101R, 2207.

[7] R. K. Swank, "Absorption and noise in X-ray phosphors," *Journal of Applied Physics*, vol. 44, no. 9, pp. 4199–4203, 1973.

[8] K. Taguchi, "Energy-sensitive photon counting detector-based X-ray computed tomography," *Radiological physics and technology*, vol. 10, no. 1, pp. 8–22, 2017.

[9] MULTiX, "X-ray spectrometric imaging," *http://www.multixdetection.com/*, 2017.

[10] N. G. Anderson, A. P. Butler, and et al., "Spectroscopic (multi-energy) ct distinguishes iodine and barium contrast material in mice," *European Radiology*, vol. 20, no. 9, 2010.

[11] H. Gao, H. Yu, S. Osher, and G. Wang, "Multi-energy ct based on a prior rank, intensity and sparsity model (prism)," *Inverse Problems*, vol. 27, no. 11, 2011.

[12] Q. Yang, W. Cong, Y. Xi, and G. Wang, "Spectral X-ray CT image reconstruction with a combination of energy-integrating and photon-counting detectors," *PLoS One*, vol. 11, no. 5, 2016.

[13] S. Feuerlein, E. Roessl, R. Proksa, G. Martens, O. Klass, M. Jeltsch, V. Rasche, H. Brambs, M. Hoffmann, and J. Schlomka, "Multienergy photon-counting k-edge imaging: potential for improved luminal depiction in vascular imaging," *Radiology*, vol. 249, no. 3, pp. 1010–1016, 2008.

[14] A. Macovski, *Medical imaging systems*. Prentice Hall, 1983.

[15] M. J. Berger, J. Hubbell, S. Seltzer, J. Chang, J. Coursey, and R. S. D. Zucker, "XCOM: Photon cross sections database," *National Institute of Standards and Technology (NIST). Available at http://physics.nist.gov/xcom*, 2007.

[16] Y. Boykov, O. Veksler, and R. Zabih, "Fast approximate energy minimization via graph cuts," *IEEE Transactions on pattern analysis and machine intelligence*, vol. 23, no. 11, pp. 1222–1239, 2001.

Author Biography

Parisa Babaheidarian received the B.Sc. degree in electrical engineering from University of Tehran in 2008. She graduated with the M.Sc. degree in electrical engineering from Sharif University of Technology in 2011, and the Ph.D. degree in electrical engineering from Boston University in January, 2018. She is currently working at Qualcomm, Inc. in Boxford, MA. Her research interests include image recognition, wireless communication, signal processing, machine learning, and information theory.

David Castañón is Professor of Electrical and Computer Engineering at Boston University. He received his Ph.D. in Applied Mathematics from MIT (1976). He was Chief Scientist at ALPHATECH before joining Boston University (1990). He has been ECE Department Chair, co-director of the Center for Information and Systems Engineering, President of the IEEE Control Systems Society, and member of Air Force Scientific Advisory Board. His interests include control, estimation, optimization, inverse problems and image understanding.